

Feed-forward Disturbance Compensation for Station Keeping in Wave-dominated Environments

Kyle L. Walker*, Adam A. Stokes*, Aristides Kiprakis† and Francesco Giorgio-Serchi*‡

*Institute for Integrated Micro and Nano Systems

†Institute for Energy Systems

School of Engineering

University of Edinburgh

Edinburgh, UK

‡Correspondence: *F.Giorgio-Serchi@ed.ac.uk*

Abstract—When deploying robots in shallow ocean waters, wave disturbances can be significant, highly dynamic and pose problems when operating near structures; this is a key limitation of current control strategies, restricting the range of conditions in which subsea vehicles can be deployed. To improve dynamic control and offer a higher level of robustness, this work proposes a Cascaded Proportional-Derivative (C-PD) with Feed-forward (FF) control scheme for disturbance mitigation, exploring the concept of explicitly using disturbance estimations to counteract state perturbations. Results demonstrate that the proposed controller is capable of higher performance in contrast to a standard C-PD controller, with an average reduction of $\approx 48\%$ witnessed across various sea states. Additional analysis also investigated performance when considering coarse estimations featuring inaccuracies; average improvements of $\approx 17\%$ demonstrate the effectiveness of the proposed strategy to handle these uncertainties. The proposal in this work shows promise for improved control without a drastic increase in required computing power; if coupled with sufficient sensors, state estimation techniques and prediction algorithms, utilising feed-forward compensating control actions offers a potential solution to improve vehicle control under wave-induced disturbances.

Index Terms—Feed-forward Control, Disturbance Compensation, State Estimation, Dynamic Control, Underwater Vehicles.

I. INTRODUCTION

ADVANCED control of marine vehicles is sharply becoming an industrial necessity rather than an academic exercise, with the offshore sector seeking higher levels of autonomy with respect to intervention tasks, inspection tasks and similar [1]. An industry section where increased autonomy would be highly beneficial is offshore, in particular the marine renewable sector, as the transition to cleaner energy sources begins to accelerate and harsher environments become the subject of exploration for power generation [2]. Remotely Operated Vehicles have become a solidified aspect of many subsea procedures, but operation near the free-surface or in shallower waters remains a challenge when the sea state is not calm, owing to the significant influence of surface waves which often limits the deployment of piloted strategies [3]. Specifically with respect to marine renewable devices, situation within a turbulent environment is critical to generate

sufficient power; thus, a greater level of robustness, reliability and precision is required with regards to vehicle control if autonomous operation is to become a reality [4].

Attempts to develop automatic disturbance compensation control algorithms have varied, with early implementations investigating vision-based solutions [5], [6]. In calmer environments these strategies can be effective, but there is a lack of robustness due to the dependence on visibility and being feedback based. To tackle this, alternative solutions have suggested inherently robust methods in the form of sliding mode and adaptive controllers [7], [8], which account for hydrodynamic loading by considering this as a set of generalised system disturbances. For small-magnitude disturbances this can improve performance sufficiently, but a question remains over stability and performance guarantees when loading increases, for example low-depth operation under large wave heights.

Handling time-varying and unsteady disturbances remains an open challenge, but a proposition which holds promise lies in exploiting forecasting methods [9], [10]; for wave-induced disturbances which are largely predictable in nature, utilising preview information can assist in disturbance compensation [11]. Given that wave predictions can be deduced through time-history data, this lends itself to being applicable to a wider range of disturbances than other proposals. Furthermore, the development of state estimation methods [12] coupled with a hydrodynamic loading model [13], [14] allows the formulation of a feed-forward (FF) control action to reduce state error, in conjunction with an established feedback controller for set-point regulation. Likewise, the formulation of a single additional control action ensures computation requirements remain low, a major benefit in relation to alternative predictive solutions [15] for these highly dynamic scenarios.

With respect to the above, this work proposes the use of a Feed-Forward (FF) control element which models the wave disturbances as a product of added inertia and hydrodynamic drag, coupling this with a Cascaded Position-Velocity Proportional-Derivative Controller (C-PD) to counteract wave disturbances. The vehicle state is estimated through an Extended Kalman Filter (EKF), which determines the corrective control action in the feedback loop. The controller is simulated under several wave conditions when the disturbance estimation

is both well-known and features significant uncertainty, showing that the proposed FF+C-PD controller outperforms a standard C-PD controller in all cases. These findings demonstrate that even coarse predictions of environmental disturbances can prove useful in mitigating state error of subsea vehicles, thus improving the accuracy of dynamic control tasks.

II. MODELLING

Throughout this work, the vehicle is considered to possess 3DoF and is restricted to a planar case; therefore the presented model considers the surge, heave and pitch motions only. Analogously, the ocean waves are modelled according to 2nd-order planar theory and are assumed to propagate unidirectionally.

A. Vehicle Rigid-Body Dynamics

The kinematics of the rigid-body are described by considering two co-ordinate frames; the earth-fixed and body-fixed. As depicted in Fig. 1, these are related by a transformation according to [18]:

$$\dot{\eta} = \mathbf{J}(\eta)\boldsymbol{\nu} \quad (1)$$

where η is a state vector describing the position and orientation of the vehicle, $\boldsymbol{\nu}$ is a state vector of linear and angular velocities and $\mathbf{J} \in \mathbb{R}^{3 \times 3}$ is the transformation matrix relating the two frames.

Given the above kinematic representation, the vehicle dynamics exhibit nonlinear behaviour and are defined according to:

$$\mathbf{M}\dot{\boldsymbol{\nu}} + \mathbf{C}(\boldsymbol{\nu})\boldsymbol{\nu} + \mathbf{D}(\boldsymbol{\nu})\boldsymbol{\nu} + \mathbf{g}(\eta) = \boldsymbol{\tau} + \boldsymbol{\tau}_E \quad (2)$$

where $\mathbf{M} = \mathbf{M}_{RB} + \mathbf{M}_A \in \mathbb{R}^{3 \times 3}$ is an inertia matrix, $\mathbf{C}(\boldsymbol{\nu}) = \mathbf{C}_{RB}(\boldsymbol{\nu}) + \mathbf{C}_A(\boldsymbol{\nu}) \in \mathbb{R}^{3 \times 3}$ is a matrix of Coriolis and centripetal terms, $\mathbf{D}(\boldsymbol{\nu}) = \mathbf{D}_L(\boldsymbol{\nu}) + \mathbf{D}_Q(\boldsymbol{\nu}) \odot |\boldsymbol{\nu}| \in \mathbb{R}^{3 \times 3}$ is a hydrodynamic damping matrix and $\mathbf{g}(\eta) \in \mathbb{R}^3$ is a vector of hydrostatic restoring forces. In the above, subscripts $_{RB}$ and $_A$ relate to contributions from rigid body and added inertial effects, with:

$$\mathbf{M}_{RB} = \begin{bmatrix} m & 0 & 0 \\ 0 & m & 0 \\ 0 & 0 & I_y \end{bmatrix} \quad \mathbf{M}_A = \begin{bmatrix} X_{\dot{u}} & 0 & X_{\dot{q}} \\ 0 & Z_{\dot{w}} & 0 \\ M_{\dot{u}} & 0 & M_{\dot{q}} \end{bmatrix} \quad (3)$$

where m is the vehicle dry mass, I_y is a rotational inertia and $X_{\dot{q}}$, $Z_{\dot{w}}$, and $X_{\dot{u}} = M_{\dot{u}}$ are added mass coefficients. The Coriolis and centripetal terms are derived in accordance with Eq. 3 [18] and the damping matrix is specified as:

$$\mathbf{D}_L = \begin{bmatrix} X_u & 0 & 0 \\ 0 & Z_w & 0 \\ 0 & 0 & M_q \end{bmatrix} \quad \mathbf{D}_Q = \begin{bmatrix} X_{u|u|} & 0 & 0 \\ 0 & Z_{w|w|} & 0 \\ 0 & 0 & M_{q|q|} \end{bmatrix} \quad (4)$$

where X_u , Z_w and M_q are linear damping coefficients whilst $X_{u|u|}$, $Z_{w|w|}$ and $M_{q|q|}$ are quadratic damping coefficients. All hydrodynamic parameters are defined in Table II.

Finally, $\boldsymbol{\tau} \in \mathbb{R}^3$ is a vector of control forces and moments whilst environmental disturbances are lumped within the vector $\boldsymbol{\tau}_E \in \mathbb{R}^3$. As this work is concerned with mitigating the effects of surface waves on vehicle behaviour, disturbances

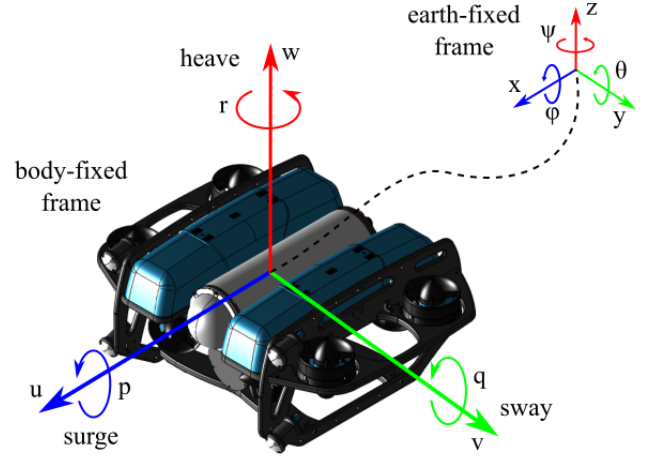


Fig. 1: The two frames, earth-fixed and body-fixed, and the relating transformation for the BlueROV2 Heavy configuration.

arising from ocean currents are assumed negligible and $\boldsymbol{\tau}_E$ is formulated to purely describe wave-induced loading, according to the model presented in the following section.

B. Wave-Induced Disturbances

To form a temporal history of the wave elevation, a 2nd-order model was adopted utilising the principle of superposition. The sea state is therefore described by a spectrum of N monochromatic components, each with a unique wave amplitude A , wave period, T , and phase offset ϵ . It follows that at a point x and at time t the wave elevation is described by [18]:

$$\zeta(x, t) = \sum_{i=0}^N A_i \cos(\kappa_i x - \omega_i t + \epsilon_i) + \sum_{i=1}^N \frac{1}{2} \kappa_i A_i^2 \cos 2(\kappa_i x - \omega_i t + \epsilon_i) \quad (5)$$

where κ and ω are the wave number and circular frequency respectively. These additional parameters are deduced by solving the dispersion relation:

$$\omega_i = \sqrt{g \kappa_i \tanh \kappa_i d} \quad (6)$$

where g and d are the gravitational constant and approximate seabed depth. In Eq. 5, the wave amplitude is related to the spectral density function $S(\omega)$ by $A^2 = 2S(\omega)\Delta\omega$ where $\Delta\omega$ is the difference between successive frequencies. Several models exist to describe the spectral density function [18]; in this work the JONSWAP spectrum is adopted owing to the relation with the North Sea, an area of interest for this application. The spectral density function is therefore:

$$S(\omega) = \frac{\alpha g^2}{\omega^5} \exp \left[-\frac{5}{4} \left(\frac{\omega_p}{\omega} \right)^4 \right] \gamma^\Gamma \quad (7)$$

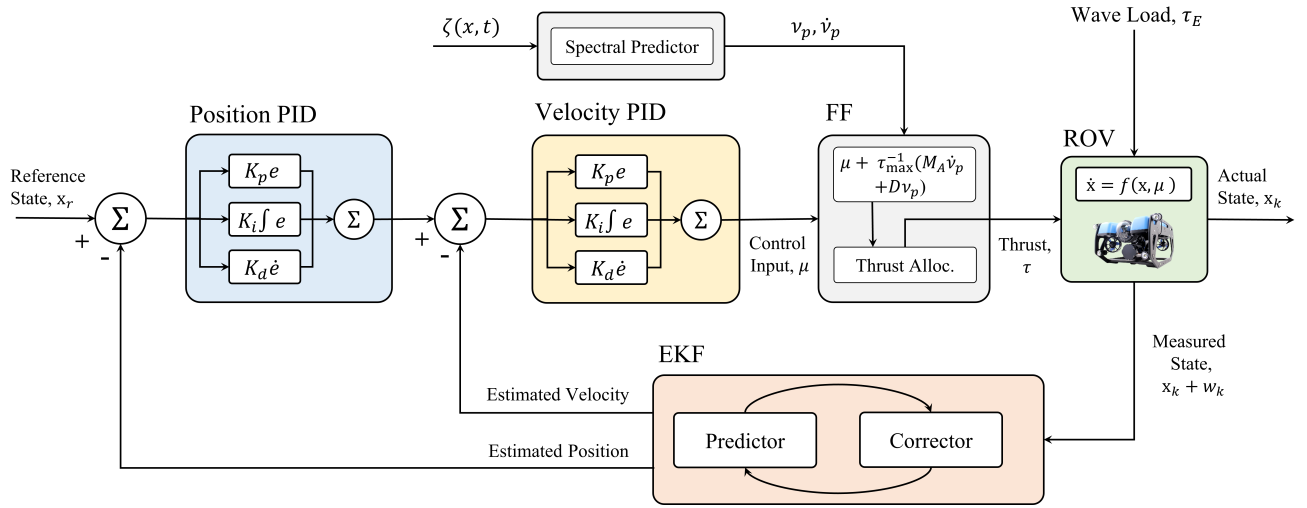


Fig. 2: Block diagram of the proposed feed-forward disturbance mitigation technique, with the grey blocks representing the generation of the additional compensating control actions.

where ω_p is the spectral peak frequency, γ^Γ is a peak enhancement factor and

$$\alpha = 0.0081$$

$$\sigma = \begin{cases} 0.07, & \text{if } \omega \leq \omega_p \\ 0.09, & \text{if } \omega \geq \omega_p \end{cases}$$

$$\Gamma = \exp \left[\frac{(\omega - \omega_p)^2}{2\omega_p^2\sigma^2} \right]$$

Spectral information can also be exploited to deduce the fluid particle motions at a point beneath the surface z , which for 2nd-order theory produces [19]:

$$u_p(x, z, t) = \sum_{i=1}^N \frac{gH_i}{2c} \frac{\cosh \kappa_i(z+d)}{\cosh \kappa_i d} \cos(\kappa_i x - \omega_i t + \epsilon_i) + \frac{3}{16} c \kappa_i^2 H_i^2 \frac{\cosh[2\kappa_i(z+d)]}{\sinh^4 \kappa_i d} \cos[2(\kappa_i x - \omega_i t + \epsilon_i)] \quad (8)$$

$$w_p(x, z, t) = \sum_{i=1}^N \frac{gH_i}{2c} \frac{\sinh \kappa_i(z+d)}{\cosh \kappa_i d} \sin(\kappa_i x - \omega_i t + \epsilon_i) + \frac{3}{16} c \kappa_i^2 H_i^2 \frac{\sinh[2\kappa_i(z+d)]}{\sinh^4 \kappa_i d} \sin[2(\kappa_i x - \omega_i t + \epsilon_i)] \quad (9)$$

where c is celerity, defined according to seabed depth to wavelength ratio [20]. This facilitates deduction of the wave-induced hydrodynamic loads (X_E , Z_E and M_E for the surge, heave and pitch respectively) acting on the body; here, a low-order model is employed which has been experimentally validated in previous work [13], [14], [22], [23]:

$$\tau_E = \begin{bmatrix} X_E \\ Z_E \\ M_E \end{bmatrix} = \begin{bmatrix} X_{\dot{u}} \dot{\nu}_{p,x} + \{X_u + X_{u|u}\} \nu_{p,x} \\ Z_{\dot{w}} \dot{\nu}_{p,z} + \{Z_w + Z_{w|w}\} \nu_{p,z} \\ \int_{-L/2}^{L/2} Z_E(x', z', t) x' dx \end{bmatrix} \quad (10)$$

where $\nu_p = [\nu_{p,x}, \nu_{p,z}]^T = \mathbf{R}_y(\theta) [u_p, w_p]^T$ ($\mathbf{R}_y(\theta)$ is a rotation matrix). Also, L is the vehicle body length and (x', z') refers to points along the vehicle axial length within the local frame.

III. CONTROL METHODOLOGY

Obtaining spectral knowledge of the immediate ocean environment around the vehicle is key in deducing the magnitude of disturbances when applying the model described by Eq. 10. Several methods have been proposed for predicting impending waves and wave loads, including but not limited to *in-situ* sensor fusion [16], auto-regressive models [9] and deterministic methods [10], the latter in particular focusing on utilising spectral information. These have been applied successfully in the context of wave energy converters, therefore an analogous deployment with respect to an underwater vehicle holds adjacent potential. It is therefore postulated here that exploiting knowledge of wave disturbances to formulate a feed-forward control action can assist in reducing state perturbations, improving station keeping performance and widening the range of deployable conditions. The control law is therefore formulated as a Cascaded Proportional-Derivative (C-PD) with feed-forward (FF) action:

$$\tau = \underbrace{\tau_{max} [\mathbf{K}_{p,v} \{\nu - (\mathbf{K}_p \mathbf{e} + \mathbf{K}_d \dot{\mathbf{e}})\}]}_{C-PD} + \underbrace{\{\mathbf{M}_A \dot{\nu}_p + \mathbf{D}(\nu_p)(-\nu_p)\}}_{FF} \quad (11)$$

where \mathbf{K}_p and \mathbf{K}_d are the position PD gains, $\mathbf{K}_{p,v}$ is the velocity P-gain and \mathbf{e} is the state error. Also, $\tau_{max} \in \mathbb{R}^3$ is a vector describing the maximum torque available in each DoF. As the heave and pitch states are controlled via the horizontal thrusters, a thrust allocation algorithm is embedded within the control architecture to generate the appropriate control inputs

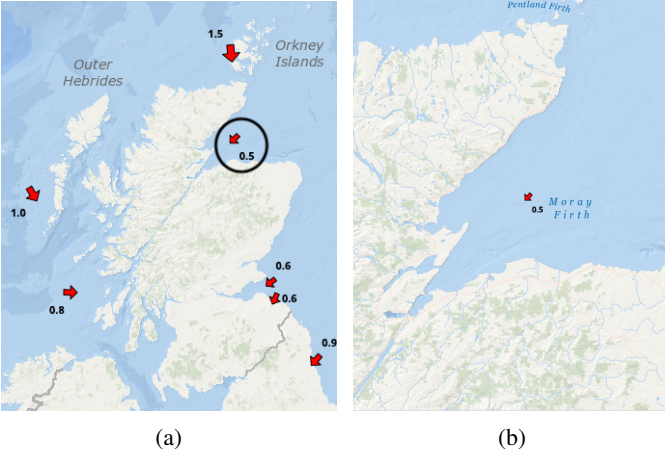


Fig. 3: Map showing the (a) various locations of buoys around Scotland, circling the buoy selected for this analysis and (b) an enlarged map of the Moray Firth buoy location.

to deliver the required forces and moments. Inclusion of the motor time-delay as a first-order response yields:

$$\boldsymbol{\mu} = \left[\left(1 - e^{-\Delta t/t_m} \right) \mathbf{K}_\tau^{-1} \right] \mathbf{B}_\mu^\dagger \boldsymbol{\tau} \quad (12)$$

where \mathbf{B}_μ^\dagger is the Moore-Penrose pseudo-inverse of the thrust allocation matrix \mathbf{B}_μ , \mathbf{K}_τ is a force co-efficient matrix and Δt_m is the motor-time constant. Eq. 12 produces a solution $\boldsymbol{\mu} \in \mathbb{R}^8$ to be allocated to each thruster.

A. State Estimation

Deploying automatic control in practice requires knowledge of the vehicles location to be known or at minimum a reasonable estimation to be inferred; to add an additional layer of realism to the simulations, we employ an EKF as a state estimator to track the vehicle state. The EKF algorithm has two update phases; the *predictor* phase and the *corrector* phase. The predictor phase considers the initial estimates and projects the error covariance and state, \mathbf{P} and $\hat{\mathbf{x}}$, ahead in time such that:

$$\mathbf{P}_k^- = \mathbf{A}_k \mathbf{P}_{k-1} \mathbf{A}_k^T + \mathbf{Q}_{k-1} \quad (13)$$

$$\hat{\mathbf{x}}_k^- = F(\hat{\mathbf{x}}_{k-1}, \boldsymbol{\mu}_{k-1}, \mathbf{w}) \quad (14)$$

where $\mathbf{A} = \frac{dF}{dx}|_{\mathbf{x}=\hat{\mathbf{x}}}$ is the linearised state transition matrix, \mathbf{Q} is the process error covariance and \mathbf{w} represents the process noise. Here, F represents a nonlinear function for the vehicle dynamics. From this, the corrector phase proceeds to compute the Kalman gain:

$$\mathbf{K}_k = \mathbf{P}_k^- \mathbf{H}_k^T (\mathbf{H}_k \mathbf{P}_k^- \mathbf{H}_k^T + \mathbf{R}_k)^{-1} \quad (15)$$

where \mathbf{H}_k is a positional measurement and \mathbf{R}_k is the measurement error covariance, before updating the estimate with a measurement y_k

$$\hat{\mathbf{x}}_k = \hat{\mathbf{x}}_k^- + \mathbf{K}_k (y_k - \mathbf{H}_k \hat{\mathbf{x}}_k^-) \quad (16)$$

TABLE I: Case assignments and parameters for the analysed wave spectra.

Case Reference	Peak Period (s)	Significant Wave Height (m)
W1	7.1	2.78
W2	9.5	3.47
W3	11.1	3.24

TABLE II: BlueROV2 Heavy dimensions and hydrodynamic parameters; data based on [24]–[26].

Parameter	Nomenclature	Value
Weight	W	112.8 N
Buoyancy	B	114.8 N
Rotational Inertia, y	I_y	0.253 kgm ²
Added Inertia Coeff.	$X_{\dot{u}}, Z_{\dot{w}}$	6.36, 18.68 kg
"	$M_{\dot{q}}$	0.135 kgm ²
"	$X_{\dot{q}}, M_{\dot{u}}$	0.67 kgm
Linear Drag Coeff.	X_u, Z_w	13.7, 33 kg/s
"	M_q	0.80 kgm ² /s
Quadratic Drag Coeff.	$X_{u u }, Z_{w w }$	141, 190 Ns ² /m ²
"	$M_{q q }$	0.47 Nms ²
Centre of Buoyancy	r_B	[0, 0, 0.028]m
Maximum Thrust	T_{max}	35 N
Thruster Offset	α	45°

Similarly, the error covariance is also corrected in this stage before looping back to Eq. 13 and repeating for every time-step k , where \mathbf{I} is an identity matrix:

$$\mathbf{P}_k = (\mathbf{I} - \mathbf{K}_k \mathbf{H}_k) \mathbf{P}_k^- \quad (17)$$

IV. SCENARIO CONFIGURATION

Given the intended application of the proposed disturbance mitigation method is for improved performance during inspection and maintenance of devices/structures in wave-dominated environments, the vehicle was simulated under three different sea states to analyse performance relative to varying wave parameters. Spectral data was sourced from the online repository of the Centre for Environmental Fishes and Aquaculture Science (Cefas) [27], collected by a wave buoy situated off the coast of Inverness, Scotland in the Moray Firth. The location of the buoy is shown in Fig. 3 where $d = 54m$; offshore wind farms are typically located within areas of this depth [28], [29], thus emulating the conditions of a typical inspection or maintenance task. The selected wave fields and assigned case references are given in Table I with all vehicle parameters given in Table II.

The controller was tasked with performing station-keeping at a depth of $z = 5m$ and for a temporal segment of 600s with a resolution of $\Delta t = 0.05s$, exposing the vehicle to significant magnitude wave disturbances for a prolonged period of time. It should be noted here that station-keeping refers to both positional and attitude regulation, during which the controller attempts to maintain a reference set-point $\mathbf{x}_r = [x_r, z_r, \theta_r]^T$. Throughout all analysis, sensor noise is considered which is mitigated by the inclusion of an EKF to estimate the vehicle

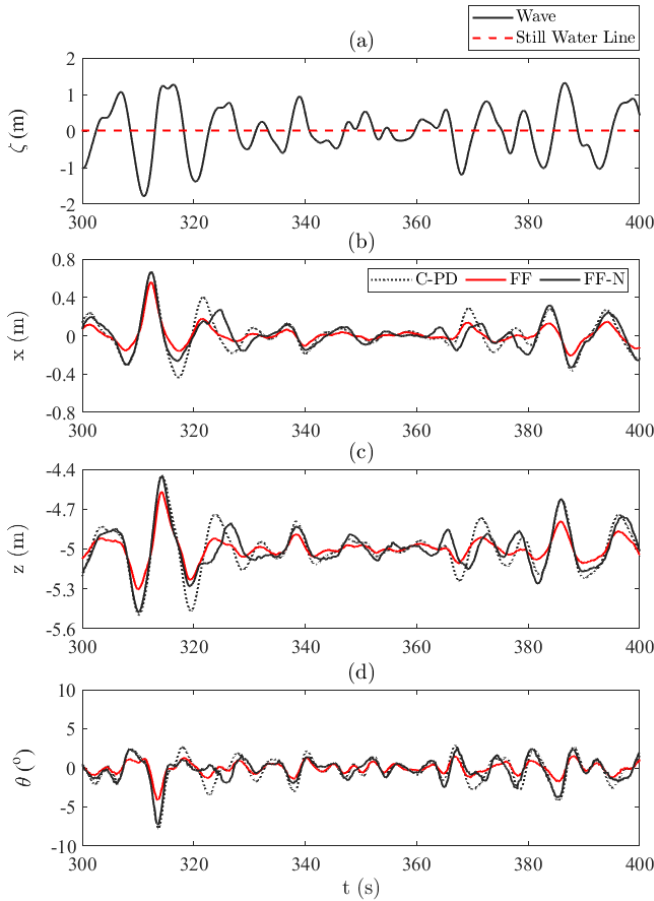


Fig. 4: Temporal segment of the (a) wave in case W3. showing the (b) surge position, (c) heave position and (d) pitch attitude.

state. Comparisons are drawn between the FF controller and a standard C-PD controller as a baseline reference which also exploits the EKF to monitor state error.

V. SIMULATION RESULTS

Performance of the proposed control scheme was analysed by considering the Root-Mean-Square-Error (RMSE) and absolute maximum error witnessed across the 600s simulation; the power consumed during the station keeping mission was also recorded and analysed.

A. Station Keeping Performance

A temporal segment for case W3 is displayed in Fig. 4 which evidently shows the FF compensation having a positive impact on the station keeping error, relative to the C-PD controller. The preview knowledge of the wave is seen to reduce RMSE by up to 58.6%, with this specific value relating to the pitch motion for case W1. For the surge and heave, the maximum reductions were also related to case W1 which returned a 47.5% and 48.2% improvement respectively. This is an indicator that for lower peak period spectra the inclusion of FF compensation is more critical, however this could be owed to the causal effect of larger pitch perturbations in contrast to cases W1 and W2.

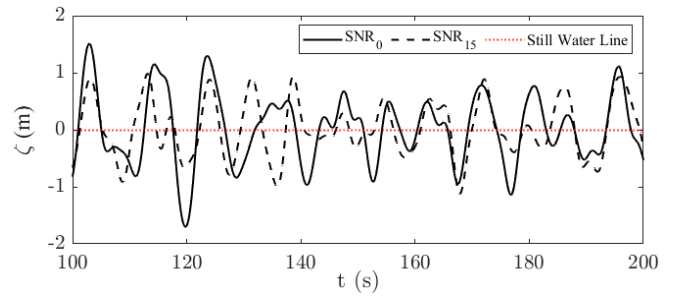


Fig. 5: Temporal segment for case W3 during noise analysis; here, SNR_0 is the encountered wave by the vehicle where as SNR_{15} is the expected wave by the controller used to generate compensating control actions.

In terms of the maximum displacement recorded during the simulations, the greatest improvement was also related to the pitch, reducing attitude error by 50.1% on average. This was much lower for the other DoF, with the surge and heave only showing 22% and 11.8% reductions; it is suspected that this is due to a brief section of the simulated waves subjecting the vehicle to sharp, high magnitude disturbances which the control was unable to correct for. Behaviour similar to this can be seen in Fig. 4 at ≈ 315 s, where the traces for the control scheme undergo similar magnitude displacements for the largest wave height in the segment. Across all cases there was a mean reduction in RMSE of $\approx 48\%$ and $\approx 28\%$ in maximum error; all absolute values are shown in Fig. 6.

B. Sensitivity to Noise

Each case was analysed when both the disturbance feed-forward term is deemed to be accurate (denoted SNR_0) and feature imprecisions (denoted SNR_{15}); the latter attempts to provide insight into controller performance when the vehicle encounters disturbances that differ from those anticipated by the FF controller. To achieve this, spectral noise with a SNR of 15 was injected directly to the spectral component amplitude and phase offset to alter the wave (and thus FF compensation calculations) significantly and randomly as shown in Fig. 5. These results are also compiled within Fig. 6.

When the disturbance is considered to be inaccurate, there is still improvement in station keeping accuracy across all cases with respect to RMSE and the majority of cases with respect to maximum error; only case W3 returns higher maximum error in the surge and heave and in these specific instances the difference is marginal with increases of $< 1\%$ and 5% respectively. The average reduction in RMSE of 17% supports the claim that these instances are at isolated periods in time and not a regular occurrence; similar to above, the pitch experienced the highest improvement in error of 14.2%. Overall these results clearly show that even utilising a spectral estimation that features inaccuracies can offer a noticeable improvement in state regulation, implying that well established methods can be applied with confidence at this end of the control pipeline.

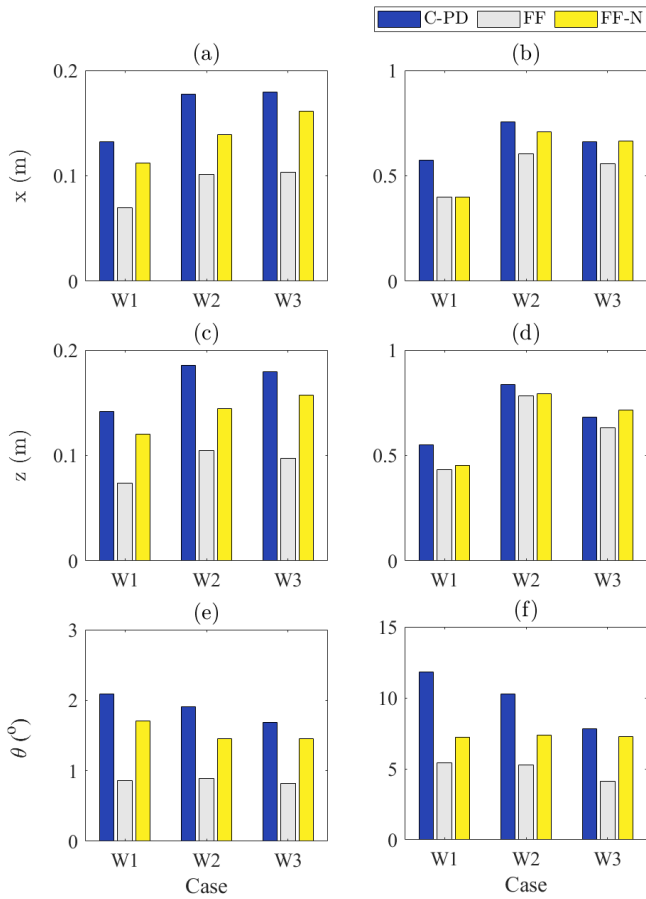


Fig. 6: State error for each control method during the station keeping simulation, showing the (a)(c)(e) RMSE and (b)(d)(f) absolute maximum error recorded.

C. Station Keeping Efficiency

Given the improvement in performance and additional control action generated by the FF component, it was anticipated additional power would be required. To confirm this, the power consumed during the mission was modelled according to manufacturer data such that [21]:

$$\mathbf{P} = 0.0011\tau^3 + 0.02078\tau^2 + 0.297\tau \quad (18)$$

where $\mathbf{P} \in \mathbb{R}^3$ is the power consumed by the control actions in each DoF. This was modelled according to a nominal operating voltage of 16V and the results are displayed in Fig. 7.

The power does increase when employing the FF scheme, but interestingly less power was consumed when considering noisy disturbance estimations. It is likely that this is attributed to the FF controller anticipating lower magnitude disturbances for the majority of the simulated mission, which would explain the increase in error that is shown in Fig. 6. Similarly, the segment displayed in Fig. 5 demonstrates this behaviour at various instances, for example at 120s where the disturbance is significantly underestimated. This supports the connected data in relation to the positional and attitude RMSE/maximum error. For large magnitude waves it can be argued that this

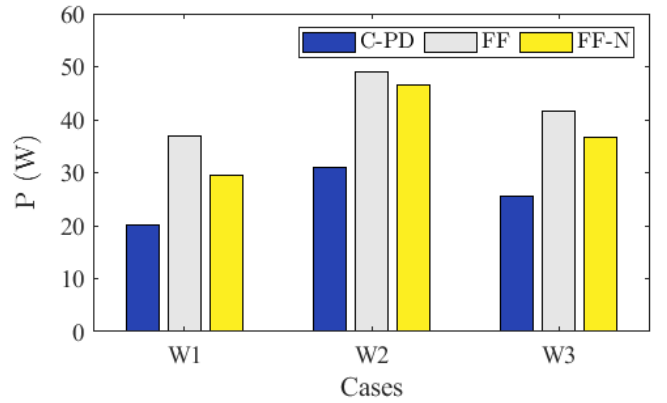


Fig. 7: Power consumed during the station keeping mission for each case and control method.

increased power expenditure is utilised well to reduce station keeping error significantly, thus in situations where this is paramount it becomes less of a burdening factor.

VI. CONCLUSIONS

This paper has proposed active wave-induced disturbance rejection for underwater vehicles based on the inclusion of a feed-forward control action. An extensive simulation study demonstrated the capability of the proposed control to significantly reduce state regulation error in both position and attitude, highlighting performance improvements of up to 56.8% over three sea states with varying parameters. Similarly, the maximum error (which is arguably the critical factor in these scenarios) was also reduced substantially, with more prominent reductions witnessed for the vehicle pitch. Given the availability of wave prediction tools, these results provide evidence of the real potential related to the incorporation of modelled wave-induced loads directly within the control to improve performance. Considering this, an interesting avenue for exploration would be to develop a preview of wave-induced disturbances along a future time-horizon; this would facilitate the development of different forms of model predictive control, potentially improving performance even further by evaluating an optimal control sequence, rather than a one step control action.

REFERENCES

- [1] H. Hastie, K. Lohan, M. Chantler, D. A. Robb, S. Ramamoorthy, R. Petrick, S. Vijayakumar and David Lane, "The ORCA Hub: Explainable Offshore Robotics through Intelligent Interfaces", arXiv preprint, 2018.
- [2] E. Zereik, M. Bibuli, N. Mišković, P. Ridaio and A. Pascoal, "Challenges and future trends in marine robotics", *Annual Reviews in Control*, vol. 46, pp. 350-368, 2018.
- [3] O. Khalid, G. Hao, C. Desmond, H. Macdonald, F. D. McAuliffe, G. Dooly and Weifei Hu, "Applications of robotics in floating offshore wind farm operations and maintenance: Literature review and trends", *Wind Energy*, vol. 25, no. 11, pp. 1880-1899, 2022.
- [4] S. Sivčev, E. Omerdić, G. Dooly, J. Coleman and Toal, D., "Towards inspection of marine energy devices using ROVs: Floating wind turbine motion replication", *Advances in Intelligent Systems and Computing*, vol. 693, 2018.

- [5] K. N. Leabourne, S. M. Rock, S. D. Fleischer and R. Burton, "Station keeping of an ROV using vision technology," *Oceans '97 MTS/IEEE Conference Proceedings*, Halifax, NS, Canada, 06-09 Oct. 1997, pp. 634-640.
- [6] R. L. Marks, H. H. Wang, M. J. Lee and S. M. Rock, "Automatic visual station keeping of an underwater robot," *Proceedings of OCEANS'94*, Brest, France, 13-16 Sept. 1994, pp. 137-142.
- [7] R. Cui, X. Zhang and D. Cui, "Adaptive sliding-mode attitude control for autonomous underwater vehicles with input nonlinearities," *Ocean Engineering*, vol. 123, 2016, pp. 45-54.
- [8] T. Elmokadem, M. Zribi and K. Youcef-Toumi, "Terminal sliding mode control for the trajectory tracking of underactuated Autonomous Underwater Vehicles," *Ocean Engineering*, vol. 129, 2017, pp. 613-625.
- [9] F. Fusco and J. Ringwood, "A Study on Short-Term Sea Profile Prediction for Wave Energy Applications", *Proc. of the 8th European Wave and Tidal Energy Conference*, Uppsala, Sweden, pp. 756-765, 2009.
- [10] M. R. Belmont, J. Christmas, J. Dannenberg, T. Hilmer, J. Duncan, J. M. Duncan and B. Ferrier, "An examination of the feasibility of linear deterministic sea wave prediction in multidirectional seas using wave profiling radar: Theory, simulation, and sea trials", *Journal of Atmospheric and Oceanic Technology*, vol. 31, no. 7, pp. 1601-1614, 2014.
- [11] X. Fang and W.-H. Chen, "Model Predictive Control With Preview: Recursive Feasibility and Stability", *IEEE Control Systems Letters*, vol. 6, pp. 2647-2652, 2022.
- [12] S. Soyly, A. A. Proctor, R. P. Podhorodeski, C. Bradley and B. J. Buckham, "Precise trajectory control for an inspection class ROV", *Ocean Engineering*, vol. 111, , pp. 508-523, 01 Jan. 2016.
- [13] K. L. Walker, R. Gabl, S. Aracri, Y. Cao, A. A. Stokes, A. Kiprakis and F. Giorgio-Serchi, "Experimental Validation of Wave Induced Disturbances for Predictive Station Keeping of a Remotely Operated Vehicle", *IEEE Robotics and Automation Letters*, vol. 6, no. 3, pp. 5421-5428, July 2021.
- [14] K. L. Walker, R. Gabl, S. Aracri, Y. Cao, A. A. Stokes, A. Kiprakis and F. Giorgio-Serchi, "Experimental Validation of Unsteady Wave Induced Loads on a Stationary Remotely Operated Vehicle", *Proc. of IEEE International Conference on Robotics and Automation (ICRA)*, Xi'an, China, pp. 2242-2248, 30 May - 05 June 2021.
- [15] D. C. Fernández, and Geoffrey A. Hollinger, "Model Predictive Control for Underwater Robots in Ocean Waves," *IEEE Robotics and Automation Letters*, vol. 2, no. 1, pp. 88-95, 2016.
- [16] J. M. Selvakumar and T. Asokan, "Station keeping control of underwater robots using disturbance force measurements", *Journal of Marine Science and Technology*, vol. 21, pp. 70-85, 2016.
- [17] C. Long, X. Qin, Y. Bian and M. Hu, "Trajectory tracking control of ROVs considering external disturbances and measurement noises using ESKF-based MPC", *Ocean Engineering*, vol. 241, 2021.
- [18] T. I. Fossen, "Guidance and Control of Ocean Vehicles", *Wiley*, Chichester, UK, 1994.
- [19] M. E. McCormick, "Ocean Engineering Mechanics with Applications", *Cambridge University Press*, New York, USA, 2010.
- [20] D. Reeve, A. Chadwick and C. Fleming, "Coastal Engineering: Processes, Theory and Design Practice", *Spon Press*, London, UK, 2004.
- [21] "T200 Thruster Datasheet," Tech. Rep. [Online]. Available: <http://docs.bluerobotics.com/thrusters/t200/d-model>
- [22] R. Gabl, T. Davey, Y. Cao, Q. Li, B. Li, K. L. Walker, et al., "Experimental force data of a restrained ROV under waves and current", *Data*, vol. 5, no. 3, pp. 57, Jun. 2020.
- [23] R. Gabl, T. Davey, Y. Cao, Q. Li, B. Li, K. L. Walker, et al., "Hydrodynamic loads on a restrained ROV under waves and current", *Ocean Engineering*, vol. 234, 15 Aug. 2021.
- [24] M. von Benzon, F. Sørensen, J. Liniger, S. Pedersen, S. Klemmensen and K. Schmidt, "Integral Sliding Mode Control for a Marine Growth Removing ROV with Water Jet Disturbance," *Proc. of 2021 European Control Conference (ECC)*, Delft, Netherlands, pp. 2265-2270, 29 June - 02 July 2021.
- [25] Blue Robotics, "BlueROV2: The world's most affordable high-performance ROV", *BlueROV2 datasheet*, Jun. 2016 [Revised Jun. 2019].
- [26] C. J. Wu, "6-DoF Modelling and Control of a Remotely Operated Vehicle", M.Eng. Thesis, College of Science and Engineering, Flinders University, 2018.
- [27] *Wave Spectra Dataset: Feb-May 2021, Moray Firth WaveNet Site*, Centre For Environment Fisheries and Aquaculture Science (Ce-fas) Online Repository, downloaded July 2022. [Online]. Available: <https://www.cefas.co.uk/data-and-publications/wavenet/>.
- [28] Bailey H, Brookes K and Thompson P (2014) Assessing Environmental Impacts of Offshore Wind Farms: Lessons Learned and Recommendations for the Future. *Aquatic Biosystems*, 10(8).
- [29] Oh KY, Nam W, Ryu M S, Kim JY and Epureanu B I (2018) A review of foundations of offshore wind energy converters: Current status and future perspectives. *Renewable and Sustainable Energy Reviews*, 88: 16-36.